INTERNATIONAL JOURNAL FOR NUMERICAL METHODS IN FLUIDS, VOL. 14, 241–251 (1992)

COMPUTATION OF AXISYMMETRIC CONFINED JETS IN A DIFFUSER

J. ZHU AND W. RODI

Institute for Hydromechanics, University of Karlsruhe, Postfach 6980, D-7500 Karlsruhe 1, F.R.G.

SUMMARY

The paper reports on a numerical study of turbulent confined jets in a conical duct with a 5° divergence. The flow has a large ratio of jet to ambient velocities at the entrance so that it gives rise to strong recirculation. The calculations are carried out with a general finite volume method designed for calculating incompressible elliptic flows with complex boundaries. Turbulence is simulated by the standard k–ε model. The sensitivity of the solution to numerical discretization errors is examined using three convection schemes, i.e. hybrid central/upwind differencing, QUICK and SOUCUP, on two grids consisting of 68×50 and 102×82 points respectively. An examination is also made of the influence of inlet boundary conditions on the predicted flow field. The computed results are compared with experimental data for mean axial velocity, turbulent shear stress and turbulent kinetic energy profiles. It is shown that the calculations reproduce the essential features of the flow observed in the experiments.

KEY WORDS Confined jet Recirculation k–ε model QUICK SOUCUP Inlet conditions

1. INTRODUCTION

Confined jets constitute a class of turbulent shear flows of great practical importance. They occur in a number of engineering applications: the pressure rise generated by the jet entrainment acts as a pump in ejectors; the establishment of recirculating currents is essential for enhancing mixing and for stabilizing flames in combustors; and the momentum transfer between two streams of different velocities provides a way to increase the thrust of V/STOL aircraft. The increasing use of such devices calls for a general method for predicting these flows.

From the computational point of view, confined jets also present several interesting features, such as the presence of an adverse pressure gradient, recirculation with unfixed separation and reattachment locations as well as coexistence of both strong and weak shear regions, which are all difficult to calculate and sensitive to either the turbulence modelling or numerical solution procedure. For example, the use of the highly stable hybrid central/upwind differencing scheme can be seriously damaging to solution accuracy owing to a combination of high flow-to-grid skewness and low grid line density, while the higher-order schemes such as QUICK are prone to instability by generating negative values of turbulent kinetic energy in the ambient region where the turbulence level is very low. On the other hand, since widely different flows ranging from non-separating flow with weak adverse pressure gradient to recirculating flow subjected to a strong adverse pressure gradient can be generated by simply changing the inlet flow conditions, confined jets are an ideal testing ground for turbulence models.

Craya and Curtet[1,2] developed an approximate theory based on the analytical solution of simplified equations of motion. They found that confined jets in constant area ducts can be

0271–2091/92/020241–11$05.50

Received October 1990
Revised April 1991

characterized by a prameter C_t, generally termed the Craya–Curtet number in recognition of their contributions in this field. Although the Craya–Curtet number C_t is not constant in variable area ducts, its value at the entrance can still be used to characterize the inlet flow conditions. Experiments have shown that recirculation occurs in cylindrical ducts when $C_t \leqslant 0{\cdot}96$[3,4] and in a conical duct with a 5° divergence when $C_t \leqslant 1{\cdot}1$.[5,6]

A numerical investigation was carried out on confined jets in both parallel and diverging circular ducts in Reference 7. Various turbulence models were used, ranging from the standard k–ε model to second-moment closure, but it was found that the algebraic stress and Reynolds stress models did not manifest themselves to be significantly superior to the k–ε model. Calculations were compared in detail with experiments; good agreement was found for a wide range of Craya–Curtet numbers, but the results deteriorated with increase of recirculation, especially in the case of the diverging duct. However, the calculations reported in Reference 7 were based on lower-order discretization schemes and on a coarse 42 x 24 grid. It is now believed that the solutions may be contaminated to some extent by numerical diffusion at small values of C_t, which correspond to strong recirculation.

The present study continues the work reported in Reference 7. The major objective is to examine the influence of numerical discretization and inlet boundary conditions on the solution, which are the two most important error sources other than a possible weakness of the turbulence model. To this end, only the flow at $C_t = 0{\cdot}59$ is considered, for which the previous calculations gave the worst agreement with experiments. Recently, the present authors[8] proposed a composite discretization procedure for steady state flow calculations. This procedure, termed SOUCUP, combines the second-order upwind, central differencing and first-order upwind schemes, with the switch from one scheme to another being automatically controlled by a convection boundedness criterion. The primary test problem results showed that the SOUCUP scheme strictly preserves the boundedness of solutions while maintaining low numerical smearing of steep gradients. This scheme is used in the present work, together with the standard hybrid central/upwind scheme[9] and QUICK.[10] Three inlet boundary conditions at two different initial jet shear layers are given to examine their influences on the solutions. Computational accuracy is assessed through comparison with experimental data.

2. MATHEMATICAL MODEL

Governing equations

The flow considered is governed by the continuity equation and the Reynolds-averaged Navier–Stokes equations. The eddy viscosity, which relates the Reynolds stresses to the corresponding mean rates of strain, is calculated using the standard k–ε model.[11] The governing equations in non-orthogonal co-ordinates using Cartesian velocity components may be written in the general form

$$\frac{\partial}{\partial x_i}(C_i\phi - D_{i\phi}) = r^\alpha J S_\phi. \tag{1}$$

The convective coefficients C_i, the diffusion terms $D_{i\phi}$ and the source terms S_ϕ are given in Table I for different dependent variables ϕ. J is the Jacobian of the transformation between curvilinear co-ordinates x_i and Cartesian co-ordinates y_i ($i = 1, 2$). Equations (1) include both plane ($\alpha = 0$) and axisymmetric ($\alpha = 1$) forms.

Equations (1) have two important features which are worthy of mention: (i) they are of strong conservation form, in which all terms arising from the divergence operator are under differential

Table I. Form of terms in the individual equations

ϕ	$D_{1\phi}$	$D_{2\phi}$	S_ϕ
1	0	0	0
V_1	$\frac{r^\alpha \mu_e}{J}(D_1+\beta_1^1\omega_1^1+\beta_2^1\omega_1^2)$	$\frac{r^\alpha \mu_e}{J}(D_2+\beta_1^2\omega_1^1+\beta_2^2\omega_1^2)$	$-\frac{1}{J}\left(\frac{\partial}{\partial x_1}(p\beta_1^1)+\frac{\partial}{\partial x_2}(p\beta_1^2)\right)$
V_2	$\frac{r^\alpha \mu_e}{J}(D_1+\beta_1^1\omega_2^1+\beta_2^1\omega_2^2)$	$\frac{r^\alpha \mu_e}{J}(D_2+\beta_1^2\omega_2^1+\beta_2^2\omega_2^2)$	$-\frac{1}{J}\left(\frac{\partial}{\partial x_1}(p\beta_2^1)+\frac{\partial}{\partial x_2}(p\beta_2^2)\right)-2\mu_e\alpha\frac{V_2}{r^2}$
k	$\frac{r^\alpha \mu_e}{J\sigma_k}D_1$	$\frac{r^\alpha \mu_e}{J\sigma_k}D_2$	$G-\rho\varepsilon$
ε	$\frac{r^\alpha \mu_e}{J\sigma_\varepsilon}D_1$	$\frac{r^\alpha \mu_e}{J\sigma_\varepsilon}D_2$	$(C_{1\varepsilon}G-C_{2\varepsilon}\rho\varepsilon)\frac{\varepsilon}{k}$

$C_1=\rho r^\alpha(V_1\beta_1^1+V_2\beta_2^1)$, $C_2=\rho r^\alpha(V_1\beta_1^2+V_2\beta_2^2)$

$D_1=B_1^1\frac{\partial\phi}{\partial x_1}+B_2^1\frac{\partial\phi}{\partial x_2}$, $D_2=B_1^2\frac{\partial\phi}{\partial x_1}+B_2^2\frac{\partial\phi}{\partial x_2}$

$\beta_j^i=$ cofactor of $\frac{\partial y_j}{x_i}$ in J

$B_j^i=\beta_1^i\beta_1^j+\beta_2^i\beta_2^j$, $\omega_j^i=\beta_j^1\frac{\partial V_i}{\partial x_1}+\beta_j^2+\frac{\partial V_i}{\partial x_2}$, $J=\begin{vmatrix}\partial y_1/\partial x_1 & \partial y_2/\partial x_1\\ \partial y_1/\partial x_2 & \partial y_2/\partial x_2\end{vmatrix}$

$\mu_e=\mu+\mu_t$, $\mu_t=\frac{\rho C_\mu k^2}{\varepsilon}$

$$G=\frac{\mu_t}{J^2}\left[2\left(\beta_1^1\frac{\partial V_1}{\partial x_1}+\beta_1^2\frac{\partial V_1}{\partial x_2}\right)^2+2\left(\beta_2^1\frac{\partial V_2}{\partial x_1}+\beta_2^2\frac{\partial V_2}{\partial x_2}\right)^2+2\alpha J^2\left(\frac{V_2}{r}\right)^2+\left(\beta_2^1\frac{\partial V_1}{\partial x_1}+\beta_2^2\frac{\partial V_i}{\partial x_2}+\beta_1^1\frac{\partial V_2}{\partial x_1}+\beta_1^2\frac{\partial V_2}{\partial x_2}\right)^2\right]$$

$C_\mu=0{\cdot}09$, $C_{1\varepsilon}=1{\cdot}44$, $C_{2\varepsilon}=1{\cdot}92$, $\sigma_k=1{\cdot}0$, $\sigma_\varepsilon=1{\cdot}32$

operators; (ii) they do not contain second derivatives of co-ordinates (curvature terms), which are very sensitive to grid smoothness.

Boundary conditions

The flow configuration considered is shown in Figure 1 together with the notation and the co-ordinate system with $y_1=x$ and $y_2=r$. To facilitate the analysis, the flow field can be divided into the following three regions.

(1) *Potential core region* in which the jet (primary stream) discharging at a uniform velocity U_J from the nozzle of diameter d_0 remains undisturbed. The length of the potential core is about $6d_0$

(2) *Ambient region* occupied by the secondary flow issuing with a uniform velocity U_α at the entrance. The turbulence level is very low and the flow may be treated as potential in this region.

(3) *Mixing region* which is characterized by an initial high-shear layer and a continuous entrainment process until complete mixing of primary and secondary streams is achieved. Depending on the inlet value of C_t, different scenarios occur in this region: at large C_t the jet reaches the duct wall before it has consumed the ambient fluid and the flow does not

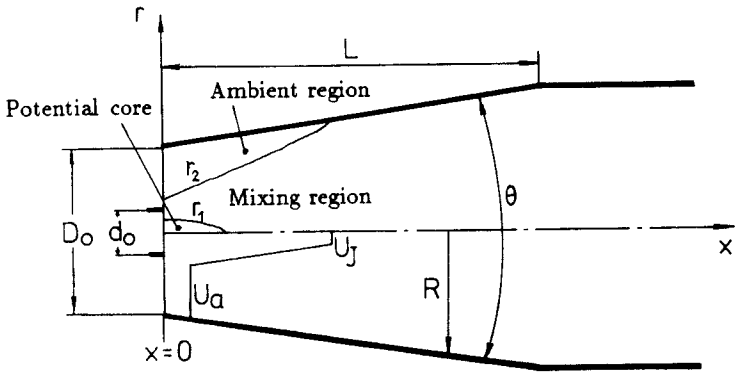

Geometry: $d_o = 1.6cm$, $D_o = 16cm$, $L = 64cm$, $\theta = 5°$.
Flow conditions: $\rho = 0.998gm/cm^3$, $\mu = 0.01gm/cm \cdot s$,
$U_J = 40cm/s$, $U_a = 2.33cm/s$.

Figure 1. Flow configuration and definitions

separate; at small C_t the jet has consumed all the ambient fluid before it reaches the wall, thereby creating reverse flow to satisfy the total mass flux conservation. After the mixing is complete, the flow degenerates eventually to the fully developed regime, if the duct is long enough, and becomes cylindrical.

The Craya–Curtet number C_t is defined by

$$C_t=\frac{1}{\sqrt{m}}, \qquad m=\frac{S}{Q^2}\int_S\left(U^2+\frac{p}{\rho}\right)\mathrm{d}S-\frac{1}{2}, \tag{2}$$

where m is the total momentum flux non-dimensionalized with the flow rate Q and the duct area S. It is shown in Reference 7 that if $d_0 \ll D_0$ and $U_a \ll W_{00}$ ($W_{00}=U_J-U_a$), C_t can be approximated by

$$C_t=\frac{U_a}{W_{00}}\frac{D_0}{d_0}. \tag{3}$$

It can be seen from this simple relation that in a given duct, recirculation may be generated and intensified by reducing the ambient flow velocity while keeping the jet velocity constant.

The computational domain sketched in Figure 1 is a diverging duct of length L followed by a cylindrical duct. Four types of boundaries are present, i.e. inlet, outlet, axis of symmetry and solid wall. The outflow boundary of the calculations is placed at $x=7{\cdot}5\,D_0$, which is sufficiently far away from the end section of the diverging duct. At this boundary the streamwise derivatives of all variables are set to zero. The calculations do not extend into the viscous sublayer near the wall, but this is bridged with the wall function approach.[11] In this the resultant wall shear stress is related to the adjacent nodal velocity component parallel to the wall by

$$\tau_w=-\lambda_w \mathbf{V}, \tag{4}$$

where

$$\lambda_w=\begin{cases}\mu/y & \text{if } y^+<11{\cdot}6,\\ \rho C_\mu^{1/4}k^{1/2}\kappa/\ln(Ey^+) & \text{otherwise,}\end{cases}$$

$$y^+=\rho C_\mu^{1/4}k^{1/2}y/\mu, \qquad \kappa=0{\cdot}4187, \qquad E=9{\cdot}0.$$

Further, the diffusive flux of k is set to zero at the wall and the value of ε at the first grid point away from the wall is determined from

$$\varepsilon = C_\mu^{3/4} k^{3/2} / \kappa y . \tag{5}$$

The inlet conditions demand special attention because they have a crucial effect on the predicted results.[12] Outside the initial jet shear layer ($r < r_1$ or $r > r_2$, where r_1 and r_2 are the co-ordinates of the inner and outer edges of the initial jet shear layer respectively) the axial velocities are given the experimental values, i.e. jet velocity $U_J = 40\ \mathrm{cm\,s^{-1}}$ and ambient velocity $U_a = 2{\cdot}33\ \mathrm{cm\,s^{-1}}$, and inside the layer the following Schlichting profile[13] is assumed

$$\frac{U - U_a}{U_J - U_a} = \left[1 - \left(\frac{r - r_1}{r_2 - r_1} \right)^{3/2} \right]^2 . \tag{6}$$

The radial velocity is set to zero. The values of k and ε, which are not available from the experiment, are specified in the following three ways.

BC1. For $r_1 < r < r_2$ (in the shear layer)

$$k = |\nu_t \partial U / \partial r| / C_\mu^{1/2}, \tag{7}$$

$$\varepsilon = C_\mu k^2 / \nu_t, \tag{8}$$

$$\nu_t = C^2 (r_2 - r_1)^2 |\partial U / \partial r|, \tag{9}$$

$$C^2 = 0{\cdot}0042 + 0{\cdot}004\, U_a / U_J; \tag{10}$$

otherwise

$$k = 10^{-5}, \qquad \varepsilon = 10^{-5}.$$

BC2. k and ε are derived from the fully developed flows in two ducts which have the same cross-sections as those of the nozzle and the annular entrance of the secondary flow.

BC3. For $0 \leqslant r \leqslant R$

$$k = \alpha_k U^2, \tag{11}$$

$$\varepsilon = \alpha_\varepsilon k^{1{\cdot}5} / d_0, \tag{12}$$

where α_k and α_ε are two adjustable constants.

Numerical solution procedure

The numerical method used to solve the system of equations (1) is a finite volume procedure designed for calculating incompressible elliptic flows with complex boundaries. It uses a non-staggered grid with all the dependent variables being stored at the same geometric centre of the control volumes. The normal-derivative diffusion terms were approximated by the central differencing scheme and the cross-derivative diffusion terms were treated explicitly as an additional source. Three discretization schemes were used to approximate the convection terms, namely hybrid central/upwind differencing,[9] QUICK[10] and SOUCUP.[8] The last two higher-order schemes were implemented in a deferred correction way proposed by Khosla and Rubin.[14]

$$\phi_i^{l+1} = \phi_i^{u,\,l+1} + \lambda (\phi_i^{h,\,l} - \phi_i^{u,\,l}), \tag{13}$$

where l indicates the iteration level, u and h represent the upwind and higher-order schemes and i refers to the ϕ-value at the cell face in question; the parameter λ blends the two schemes, with limiting values $\lambda = 0$ for the upwind and $\lambda = 1$ for the higher-order solution. The deferred

correction leads to an always diagonally dominant coefficient matrix, thus lending the necessary stability to the numerical process while restoring higher-order accuracy at convergence.

As a result the discretized counterparts of equation (1) can be cast into the following linearized form:

$$A_P \phi_P^{l+1} = \sum_i A_i \phi_i^{l+1} + S_\phi^U + S_{DC}, \tag{14}$$

where the main coefficients A_i include both the convection (calculated only by the upwind scheme) and the normal diffusion terms and the coeffcient S_ϕ^U contains the physical source S_ϕ as well as the cross-derivative diffusion terms. The extra source term S_{DC} results from the anti-diffusive part $\lambda(\phi_i^{h,l} - \phi_i^{u,l})$ of the deferred correction defined by equation (13). The resulting set of algebraic difference equations (14) was solved with the strongly implicit solution algorithm of Stone.[15] The calculation results were declared converged when the maximum normalized residue of all the dependent variables was below 0·5%. The details of the present numerical procedure are given in References 16 and 17.

All calculations were performed on a Siemens/Fujitsu VP400-EX vector computer. The computer code has been vectorized to a major extent so that high computational efficiency can be achieved. The most important part not fully vectorized is Stone's solution algorithm, which consumed more than 60% of the CPU time. Nevertheless, the total CPU time was reduced by at least a factor of 40 compared with corresponding scalar mode runs.

3. DISCUSSION OF RESULTS

Influence of numerical discretizations

Computations were first performed to examine the grid dependence of the solution. To this end, two grids with 68×50 and 102×82 points and three discretization schemes, i.e. HYBRID (central/upwind differencing), QUICK and SOUCUP, were used. Figure 2 shows the upstream part of the 68×50 grid (the total length of the computational domain is 120 cm). The grid has been refined in the vicinity of the nozzle, particularly in the radial direction, to resolve steep gradients of the jet shear layer. Test results are shown in Figure 3(a) for the decay of the centreline velocity U_0 non-dimensionalized by the mean velocity of the section, U_m, and in Figure 3(b) for the radial variation of the turbulent shear stress $\overline{uv}$ at the section $x = 30$ cm. The solutions of QUICK and SOUCUP on the fine 102×82 grid are not shown in the figures because the grid refinement from 68×50 to 102×82 produced too small differences to be seen on the graph. This means that both QUICK and SOUCUP already gave grid-independent solutions on the 68×50

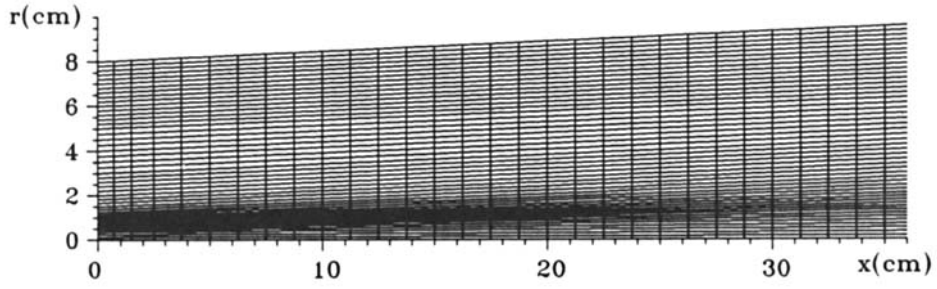

Figure 2. Grid in the upstream of the diffuser

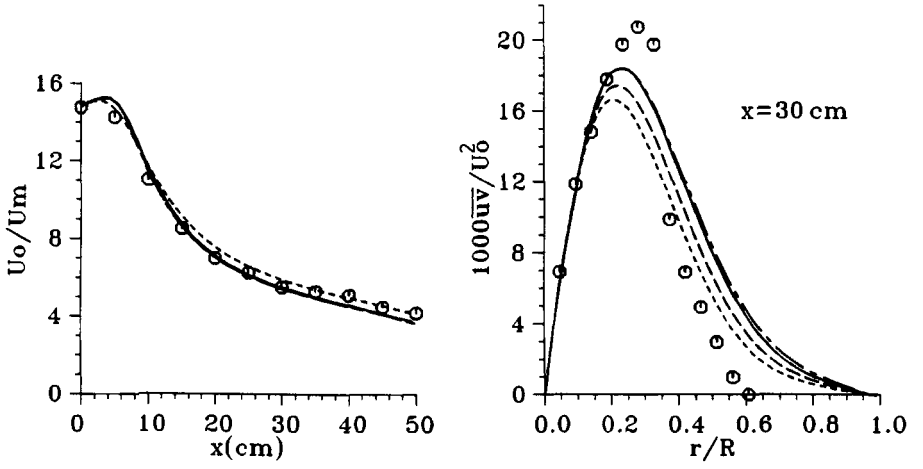

(a) Centerline velocity decay (b) Turbulent shear stress

Figure 3. Grid independence tests: ○, experiment;[5] 102 × 82 grid: – –, HYBRID; 68 × 50 grid: ———, SOUCUP; – · –, QUICK; ---, HYBRID

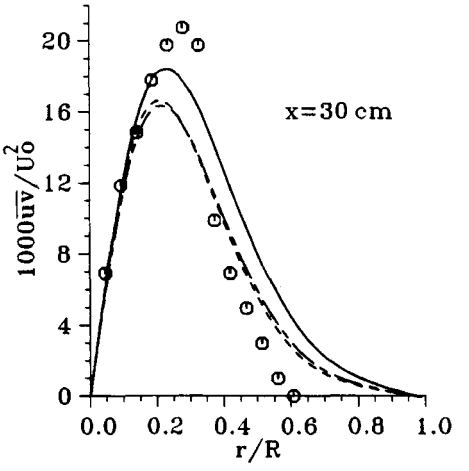

Figure 4. Turbulent shear stress: ○, experiment;[5] ———, SOUCUP (for U, V, k, ε); – – –, SOUCUP (only for U, V); – · –, HYBRID

grid. It can be seen that the results of SOUCUP are nearly the same as those of QUICK; the result of HYBRID on the fine grid reached the higher-order solutions for the centreline velocity (Figure 3(a)), but this was not so for the turbulent shear stress profile in Figure 3(b). The CPU-times in minutes required for the calculations with SOUCUP/QUICK/HYBRID were 3·3/3·5/2·7 on the 102 × 82 grid and 0·62/0·61/0·45 on the 68 × 50 grid.

In the above calculations the higher-order schemes were applied not only to the momentum equations but also to the k- and ε-equations. Since it was argued before that the use of higher-order schemes may not be necessary for the turbulence equations owing to their source-dominant

property,[18] a calculation with SOUCUP scheme being applied only to the momentum equations was made to verify whether this argument is true or not for the present flow problem. The test result for the shear stress profile at $x=30$ cm is shown in Figure 4. It can be seen that this calculation gives a result very close to that obtained with the HYBRID scheme, which shows that, at least for the flow problem considered, the turbulence equations are more sensitive to the convection scheme than the momentum equations.

Influence of inlet conditions

The sensitivity of the solution to changes in inlet conditions was examined by comparing centreline velocity decays resulting from the three different inlet conditions specified above (BC1, BC2 and BC3 with $\alpha_k=0{\cdot}01$ and $\alpha_\varepsilon=3{\cdot}65$). Two initial jet shear layer thickness $\delta=1$ and 0·1 ($\delta=2(r_2-r_1)/d_0$) were used, the former corresponding to the experimental observation and the latter to a step profile which was usually declared in experiments because details of the initial shear layer behaviour were not examined. The initial eddy viscosity distributions resulting from the various inlet conditions for turbulent quantities are depicted in Figure 5. Figures 6(a) and 6(b)

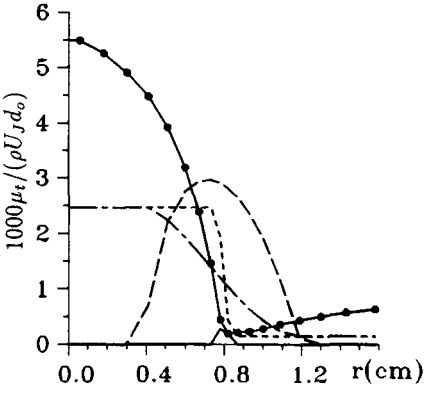

Figure 5. Initial eddy viscosity distributions: – –, BC1 ($\delta=1$); ——, BC1 ($\delta=0{\cdot}1$); —●—, BC2; ———, BC3 ($\delta=1$); - - -, BC3 ($\delta=0{\cdot}1$)

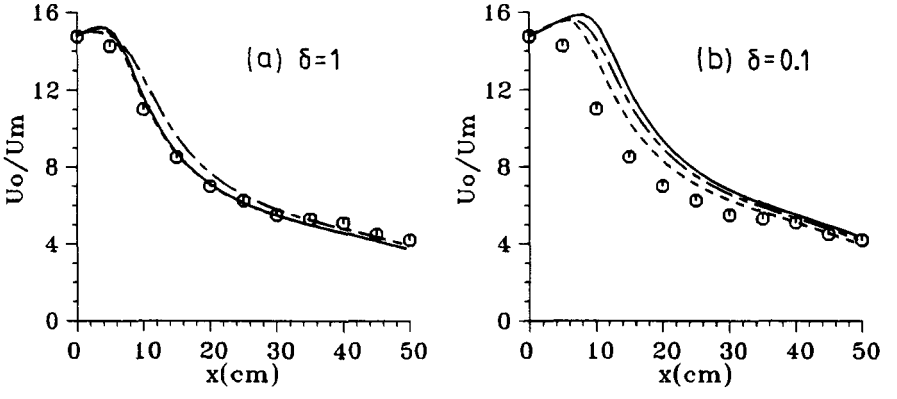

Figure 6. Centreline velocity decay: O, experiment;[5] ——, BC1; ———, BC2; - - -, BC3

show the influence of the inlet conditions on the centreline velocity decay. It can be seen that the predicted results are affected much more strongly by the initial shear layer thickness than by the turbulence conditions. The BC1 and BC3 results were very similar at $\delta = 1$, while the fully developed profiles (BC2) produced somewhat different results. The test shows that the turbulence can quickly adjust itself to a suitable level in the near-entrance region, but the jet tends to retain its core longer when the initial shear layer is thinner. It is of interest to note that the increase in the calculated non-dimensionalized centreline velocity profile in the near-entrance region (Figures 3(a) and 6) is only due to the decrease in the sectional mean velocity U_m, whereas the centreline velocity U_0 itself remains constant in the potential core.

Presentation of results

The results presented subsequently are all from the calculation with SOUCUP and the inlet condition BC1, obtained on the 68 × 50 grid. The predicted streamlines shown in Figure 7 convey an overall view of the flow pattern. It is seen that the ambient flow is sucked in by the jet in the near-entrance region and a long toroidal recirculation bubble is set up at the duct wall. Also shown in Figure 7 are the computed and measured separation and reattachement locations; good agreement between them is observed.

The predicted axial mean velocity profiles at four sections are shown and compared with the experimental data in Figure 8. The calculation is seen to yield generally good agreement with the measurement for all the sections considered. These U-profiles clearly reveal the flow evolution: the interface between the two streams is well defined and there exists a constant ambient velocity

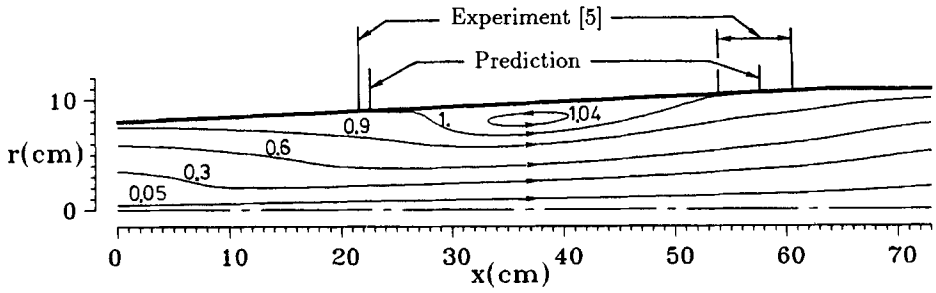

Figure 7. Predicted streamlines

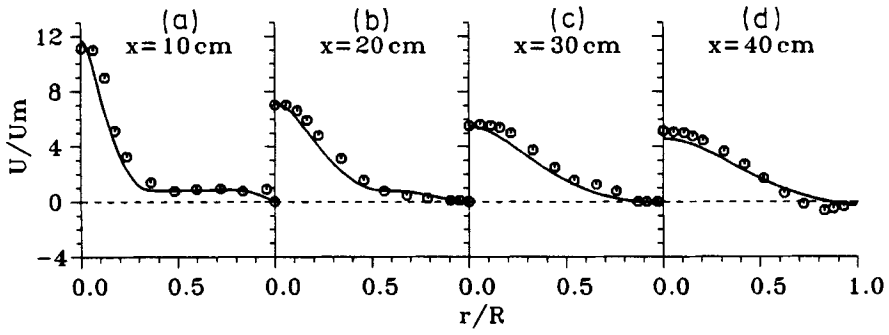

Figure 8. Axial mean velocity: O, experiment:[5] ———, calculation

at upstream locations, say $x = 10$ cm; the jet continously expands in the downstream direction and at $x = 20$ cm it has entrained almost all the ambient fluid; further downstream reverse flow occurs and the flow has completely lost the character of a jet. Figure 8(d) indicates that the calculations underpredict the width of the reverse flow region, pointing to limited accuracy of the k–ε model in this region.

Figures 9 and 10 show the computed and measured turbulent shear stress ($\overline{uv}$) and turbulent kinetic energy (k) profiles. Only measured normal stress components $\overline{uu}$ and $\overline{vv}$ were available and k was extracted from the experiments by assuming $\overline{ww} = \overline{vv}$. Comparison with the experimental data indicates that the calculation qualitatively reproduces the basic turbulence characteristics observed in the experiment, but substantial discrepancies are present for both $\overline{uv}$- and k-profiles. Since the numerical error has been reduced to a minimal level, these discrepancies must be attributed to shortcomings of the k–ε turbulence model and/or to possible experimental errors. Part of the discrepancy seen in Figure 9(d) is due to the underprediction of the width of the reverse flow region, but it seems somewhat doubtful that in the experiments the change in sign of the shear stress $\overline{uv}$ should occur much further away from the diffuser wall than the velocity minimum. The measured turbulence intensity shown in Figure 10(d) also points to some uncertainty in the recirculation region. Moreover, an apparently unsteady behaviour of the

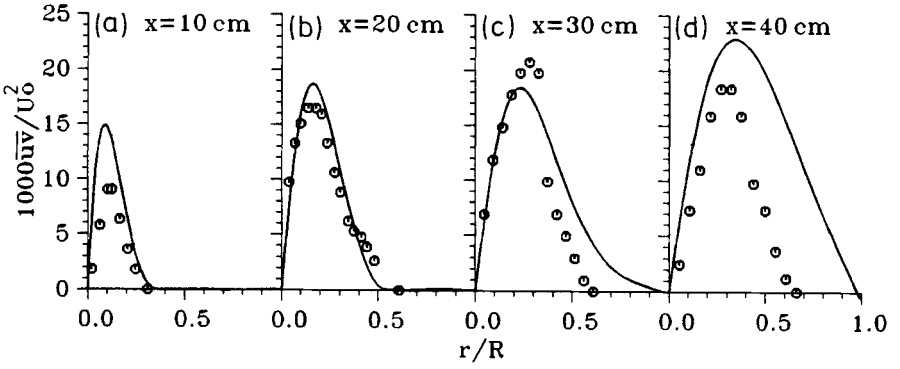

Figure 9. Turbulent shear stress: ○, experiment:[5] ———, calculation

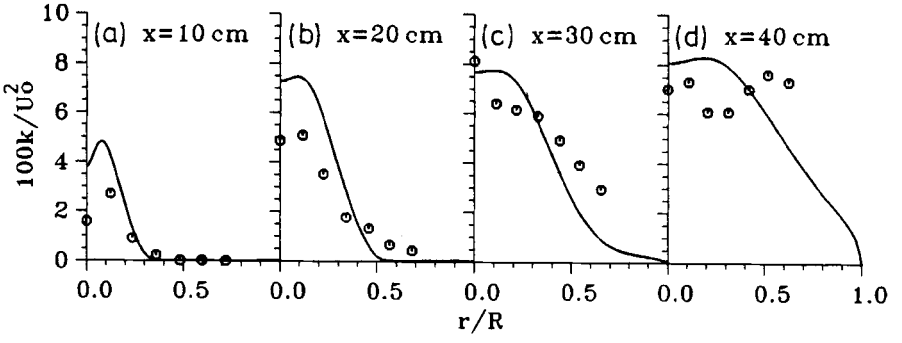

Figure 10. Turbulent kinetic energy: ○, experiment:[5] ———, calculation

recirculation bubble in the downstream region of the diffuser was observed in the experiment,[5] which cannot be simulated with the present numerical procedure.

4. CONCLUSIONS

The present study has demonstrated the importance of the use of higher-order schemes for discretizing the convection terms of transport equations. Both QUICK and SOUCUP give accurate numerical solutions already on the 68×50 grid, whereas the solution with the HYBRID scheme responds to grid refinement in a rather slow way, so that it is still far away from grid independence on the 102×82 grid. The higher-order discretization of the turbulence equations, often considered of subordinate importance, plays a crucial role in accurately simulating flows of this kind.

The calculations were found to be more sensitive to the specification of the jet shear layer thickness than to that of turbulent quantities outside the initial shear layer at the inlet. A step profile consisting of uniform jet and ambient velocities, usually declared in experiments, leads to a rather poor prediction of the upstream flow field. The calculations with the inlet conditions based on the existence of an initial shear layer (BC1) yield generally good agreement with experimental data, but the recirculation region is predicted somewhat too thin.

REFERENCES

1. A. Craya and R. Curtet, 'Sur l'évolution d'un jet en espace confiné', *C. R. Acad. Sci. Paris*, **241**, 621–622 (1955).
2. R. Curtet, *Sur l'Ecoulement d'un Jet entre Parois*, Publications Scientifiques et Techniques du Ministère de l'Air, Paris, 1960.
3. M. Barchilon and R. Curtet, 'Some details of the structure of an axisymmetric confined jet with backflow', *J. Basic Eng.*, **86**, 777–787 (1964).
4. M. Barchilon, *Contribution à l'Etude des Courants de Retour Engendrés par un Jet Confiné*, Publications Scientifiques et Techniques du Ministère de l'Air, Paris, 1969.
5. K. Kian, 'Jets confinés dans un divergent', *Thèse de Docteur-Ingénieur*, Université Scientifique et Médicale et Institut National Polytechnique de Grenoble, 1981.
6. G. Binder and K. Kian, 'Confined jets in a diverging duct', *Proc. Turbulent Shear Flows 4*, Karlsruhe, September 1983, pp. 7.18–7.23.
7. J. Zhu, 'Calcul des jets turbulents confinés avec recirculation', *Thèse de Docteur*, Institut National Polytechnique de Grenoble, 1986.
8. J. Zhu and W. Rodi, 'A low dispersion and bounded convection scheme', *Comput. Methods Appl. Mech. Eng.*, in the press.
9. D. B. Spalding, 'A novel finite difference formulation for differential expressions involving both first and second derivatives', *Int. j. numer. methods eng.*, **4**, 551–559 (1972).
10. B. P. Leonard, 'A stable and accurate convective modelling procedure based on quadratic upstream interpolation', *Comput. Methods Appl. Mech. Eng.*, **19**, 59–98 (1979).
11. B. E. Launder and D. B. Spalding, 'The numerical computation of turbulent flows', *Comput. Methods Appl. Mech. Eng.*, **3**, 269–289 (1974).
12. J. Zhu, G. Binder and J. L. Kueny, 'Improved predictions of confined jets with a parabolic computation of the entrance region', *AIAA J.*, **25**, 1141–1142 (1987).
13. H. Schlichting, *Boundary Layer Theory*, McGraw-Hill, New York, 1968.
14. P. K. Khosla and S. G. Rubin, 'A diagonally dominant second-order accurate implicit scheme', *Comput. Fluids*, **2**, 207–209 (1974).
15. H. L. Stone, 'Iterative solution of implicit approximations of multidimensional partial differential equations', *SIAM J. Numer. Anal.*, **5**, 530–558 (1968).
16. S. Majumdar, 'Development of a finite-volume procedure for prediction of fluid flow problems with complex irregular boundaries', *Report SFB 210/T/29*, University of Karlsruhe, 1986.
17. W. Rodi, S. Majumdar and B. Schönung, 'Finite-volume method for two-dimensional incompressible flows with complex boundaries', *Comput. Methods Appl. Mech. Eng.*, **75**, 369–392 (1989).
18. M. A. Leschziner and W. Rodi, 'Calculation of annular and twin parallel jets using various discretization schemes and turbulence-model variations', *J. Fluids Eng.*, **103**, 352–360 (1981).